Journal of Quantitative Spectroscopy & Radiative Transfer 347 (2025) 109658

Contents lists available at ScienceDirect

Journal of Quantitative Spectroscopy and Radiative Transfer

journal homepage: www.elsevier.com/locate/jqsrt

A novel spectroscopic design toward the measurement of electron's electric dipole moment using lead monofluoride

Zesen Wang [a], Renjun Pang [a], Jie Ma [a], Qinning Lin [a], Yabing Ji [a], Shunyong Hou [a], Xiaohu Li [b,d,e], Liang Xu [f], Xingjia Li [g], Guanglong Chen [g], Zhenghai Yang [a,c,*], Jianping Yin [a], Tao Yang [a,b,c,*]

[a] State Key Laboratory of Precision Spectroscopy, East China Normal University, Shanghai 200062, China
[b] Xinjiang Astronomical Observatory, Chinese Academy of Sciences, 150 Science 1-Street, Urumqi, Xinjiang 830011, China
[c] Collaborative Innovation Center of Extreme Optics, Shanxi University, Taiyuan, Shanxi 030006, China
[d] Xinjiang Key Laboratory of Radio Astrophysics, 150 Science 1-Street, Urumqi, Xinjiang 830011, China
[e] Key Laboratory of Radio Astronomy and Technology, Chinese Academy of Sciences, A20 Datun Road, Chaoyang District, Beijing, 100101, China
[f] Shanghai Key Lab of Modern Optical System, University of Shanghai for Science and Technology, 516, Jungong Road, Shanghai 200093, China
[g] School of Mathematics, Physics and Statistics, Shanghai University of Engineering Science, Shanghai 201620, China

ARTICLE INFO

Keywords:
Electron's electric dipole moment (eEDM)
Spectroscopic detection
Lead monofluoride (PbF)
The Standard Model

ABSTRACT

The search for the electron's electric dipole moment (eEDM) has long been pursued to explore the new physics beyond the Standard Model. To date, the most stringent constraints on the eEDM measurement were imposed by paramagnetic polar diatomic molecules/molecular ions through probing the changes of the precession rate of electron spins in an electric field, although nonzero eEDM has not been reported yet. In this study, we propose a novel design of spectroscopic detection in the lead monofluoride ($^{208}Pb^{19}F$) molecule that can take full advantage of its long coherent ground state, low Landé g factor, strong internal electric field, and unique field-dependent eEDM sensitive transition. Adopting an effective Hamiltonian approach, we untangle the complicated J-mixing energy level structure of the coherent ground state $X_1{}^2\Pi_{1/2}(v = 0, J = 1/2, e, F = 1, |M_F| = 1)$, and characterize the rotational branching ratios in the $A^2\Sigma_{1/2}(v' = 0) \leftarrow X_1{}^2\Pi_{1/2}(v = 0)$ detection scheme. We demonstrate the highly asymmetric branching ratios in the $\Sigma\leftarrow\Pi$ transition which permits the preparation of coherently mixed states, followed by the simulated Stark spectroscopy under the externally applied electric field to address the sensitive transition $Q_{fe}(1/2)$ for the eEDM measurement. In the end, we discuss the feasibility of laser cooling and Stark deceleration of PbF molecules. Our detection scheme will support us in constructing a fully optical approach toward the eEDM measurement using PbF molecules, which can enrich the molecular pool that explores the fundamental physics on a table-top apparatus.

1. Introduction

Since Purcell and Ramsey proposed that neutrons and electrons may possess an electric dipole moment (EDM) proportional to spin that violates time-reversal symmetry [1], numerous strategies have been initiated to search for new physics beyond the Standard Model such as the matter-antimatter asymmetry [2] and the origin of dark matter and dark energy [3]. The existence of nonzero electron's electric dipole moment (eEDM) can simultaneously violate the space (P) parity and time-reversal (T) parity, and has been considered in the last decades to be central to resolve these intriguing problems. Particularly, an observed eEDM value d_e at the level significantly greater than the prediction of the Standard Model ($<10^{-38}$ e·cm) [4] will directly test the extensions of the Standard Model, which predict distinct eEDM values at the typical level of 10^{-25} to 10^{-31} e·cm [5–13]. Prospective experimental and theoretical studies utilizing atoms or diatomic, triatomic, and even polyatomic molecules/molecular ions are proposed to measure the eEDM. In 2002, the eEDM measurement using thallium (Tl) atoms achieved the experimental upper limit of $d_e < 1.6 \times 10^{-27}$ e·cm in the paramagnetic atomic systems [14]. Since then, research has increasingly focused on polar molecular systems, which offer enhanced sensitivity and systematic advantages over atomic candidates due to their large internal electric

* Corresponding authors.
E-mail addresses: zhyang@lps.ecnu.edu.cn (Z. Yang), tyang@lps.ecnu.edu.cn (T. Yang).

https://doi.org/10.1016/j.jqsrt.2025.109658
Received 30 March 2025; Received in revised form 29 August 2025; Accepted 3 September 2025
Available online 4 September 2025

fields. In 2011, the experimental result of $d_e < 1.05 \times 10^{-27}$ e·cm was obtained by using the pulsed supersonic beam of YbF in its ground $X^2\Sigma^+$ state with the effective electric field (E_{eff}) of 14.5 GV/cm [15]. In 2018, the ACME collaboration made further strides and announced a new limit of $d_e < 1.1 \times 10^{-29}$ e·cm by utilizing a buffer-gas cooled beam of ThO molecules in the $H^3\Delta_1$ state with E_{eff} of 78 GV/cm and increased molecular density along with improved state preparation scheme [16,17]. Only recently, the best experimental limit of $d_e < 4.1 \times 10^{-30}$ e·cm was reported with trapped HfF^+ molecular ions [18]. These tabletop-scale experiments have unambiguously revealed new physics by imposing new constraints on potential explanations of the matter-antimatter asymmetry. Other experimental and theoretical investigations towards the eEDM measurement have been conducted involving atomic candidates of Fr [19] and Cs [20–22], solid state materials of gadolinium gallium garnet (GGG) [23] and gadolinium-iron garnet (GdIG) [24], polar molecules embedded within a rare-gas matrix such as BaF-Ar/Ne [25–28], molecular ions of ThF^+ [29–33], and diatomic candidates of BaF [37–39], WC [40–42], RaF [43], RaH [44], HgBr [45], HgH [46], CdH [47], LrO [48], and HgF [49]. Moreover, triatomic molecules/molecular ions like YbOH [50,51], HgOH [52], $AcOH^+$ [34], and $LuOH^+$ [35,36], together with polyatomic (symmetric top) molecules such as $YbOCH_3$ [53] and $RaOCH_3$ [54], are also regarded as promising candidates with laser cooling feasibility and large E_{eff}.

The $^{208}Pb^{19}F$ molecule (herein PbF) is also predicted to possess unique molecular properties for the eEDM measurement [55,56]. First, PbF is found to have an E_{eff} of about 31 GV/cm [56] thus enhancing the effect of the eEDM through a linear Stark shift of considerable magnitude. Critically, this strong internal polarization can be achieved with a modest external electric field (~ 10 kV/cm), substantially reducing experimental challenges such as the electrode precision, high-voltage breakdown and associated systematic errors. Furthermore, the ground state of PbF ($X_1{}^2\Pi_{1/2}$) ensures that the eEDM coherence time will not be limited by its lifetime, while its near-zero Landé g factor of the lowest rotational state [55] suppresses the background magnetic-field-induced systematic error. For the eEDM measurement, the $A(v' = 0) \leftarrow X_1(v = 0)$ ($Q_{fe}(1/2)$) transition (444 nm) is preferred over ultraviolet alternatives (*e.g.*, $B \leftarrow X_1$ at 280 nm) due to the cost-effectiveness of visible lasers, and the extended lifetime of the A state (5 μs) [57] narrows down the natural linewidth for enhanced spectral resolution under strong electric fields. By employing the pseudo-continuous resonance-enhanced multiphoton ionization (pc-REMPI) scheme [58] in the detection of $A(v' = 0) \leftarrow X_1(v = 0)$ transition, the signal-to-noise ratio can be significantly enhanced, while the $B \leftarrow X_1$ transition would generate higher-energy photons, inducing excessive background ion noise in REMPI detection [59].

Therefore, it is essential to investigate the preparation of eEDM-sensitive coherent states and the spectroscopy of the $A(v' = 0) \leftarrow X_1(v = 0)$ transition of PbF under external electric fields. In this work, the hyperfine structures of lowest rotational levels of $X_1{}^2\Pi_{1/2}(v = 0)$ and $A^2\Sigma_{1/2}(v' = 0)$ states, an analysis of the J-mixing and branching ratios for the eEDM-sensitive states within the $Q_{fe}(1/2)$ transition, the Stark energy levels involved in the $Q_{fe}(1/2)$ transition and their dependence on the external electric field, as well as a simulation of $Q_{fe}(1/2)$ hyperfine transition lines under different electric fields are examined theoretically. Additionally, we evaluate the feasibility of laser cooling and Stark deceleration for PbF. These investigations provide a deeper understanding of the role of PbF in realizing a sensitive eEDM measurement, thus contributing to the development of experimental approaches for heavy diatomic molecular systems that can be utilized to search for new physics beyond the Standard Model.

2. Hyperfine-resolved energy level structures of X_1 and A states

In this section, we focus on calculating the hyperfine-resolved energy level structures of X_1 and A states using the effective Hamiltonian theory, thereby defining the spectroscopic framework for subsequent eEDM-sensitive coherent state preparation. For the PbF molecule, its ground state X_1 is a $^2\Pi_{1/2}$ state with large spin-orbit coupling while the upper A state is an $\Omega = 1/2$ state with even larger Ω doubling [60] (The Ω doubling parameters for $X_1{}^2\Pi_{1/2}$ and $A^2\Sigma_{1/2}$ states are -0.138200(6) cm^{-1} and 0.6185(3) cm^{-1} respectively [61]). For computational convenience, both X_1 and A states are simulated and described within the Hund's case (a) coupling framework, with their quantum states sharing identical basis function in Eq. (1) [62]:

$$|F, I, J, M_F, p_s\rangle = \frac{1}{\sqrt{2}}\left(|F, I, J, M_F, \Omega = 1/2\rangle + p_s\,(-1)^{J-\frac{1}{2}}|F, I, J, M_F, \Omega = -1/2\rangle\right) \quad (1)$$

The effective Hamiltonian of $\mathbf{H_{eff}}$ describes all the involved intercoupling degrees of freedom in a molecular system. For PbF in the Hund's case(a), the effective Hamiltonian can be described by

$$\mathbf{H_{eff}} = \mathbf{H_{rot}} + \mathbf{H_0} + \mathbf{H_1} + \mathbf{H_{stark}}. \quad (2)$$

Here the interaction $\mathbf{H_{rot}}$ describes the spin-rotational motion of the molecule, neglecting all nuclear spins. The hyperfine structure resulting from the Frosch and Foley picture [63] of the interaction of the nuclear spin with an electron in a specified quantum orbit is depicted by $\mathbf{H_0}$. The small corrections to the hyperfine structure involving nuclear-spin-rotational and nuclear-spin-spin (bipolar) interactions are included in $\mathbf{H_1}$. Finally, $\mathbf{H_{stark}}$ describes the Stark interaction of the molecule with an electric field. The molecular parameters and the corresponding matrix representations for each term of the effective Hamiltonian $\mathbf{H_{eff}}$ with the basis set $|F, I, J, M_F, p_s\rangle$ are depicted in the Appendix. The field-free eigenvalues and eigenvectors along with the energy level structures without an external electric field of $X_1(v = 0)$ and $A(v' = 0)$ states are then obtained by numerical diagonalization of the effective Hamiltonian matrix representations (Fig. 1).

3. Branching ratios for the $Q_{fe}(1/2)$ transition

Having established the zero-field hyperfine energy level structures of X_1 and A states, we now investigate the transitions critical for eEDM-sensitive state preparation. In the proposed eEDM measurement, the eEDM phase carried by PbF molecules can be detected via spectroscopic methods such as REMPI [58] through the eEDM sensitive transition $A(|J' = \frac{1}{2}, p_s' = -1, F' = 1, M_F' = 0\rangle) \leftarrow X_1(|J = \frac{1}{2}, p_s = 1, F = 1, |M_F| = 1\rangle)$ in the external electric field E_z, while the eEDM-sensitive superposition states are expressed as $(|M_F = 1\rangle + |M_F = -1\rangle)/\sqrt{2}$. The $A(J', p_s') \leftarrow X_1(J, p_s)$ transitions can be labeled by the branches of $R_{ee}(J), R_{ff}(J), P_{ee}(J), P_{ff}(J)$, $Q_{ef}(J)$, and $Q_{fe}(J)$, respectively. Here R, P, and Q indicate transitions involving $J' = J + 1$, $J - 1$, and J respectively. The first e/f subscript determines the sign of the product $q'\chi'$ for the A state, with e indicating $q'\chi' = 1$ and f indicating $q'\chi' = -1$ respectively. Here χ' represents the total parity defined as $\chi' = \pm 1 = (-1)^{F'} p_s'$, while $q' = 2(J' - F')$ [58]. Similarly, the second e/f subscript determines the sign of the product $q\chi$ for the X_1 state. Therefore, the eEDM sensitive transition in the $A(J', p_s') \leftarrow X_1(J, p_s)$ detection scheme can be labeled as $Q_{fe}(1/2)$ for PbF molecules.

The branching ratios reflect the distributions of the transition intensities for all possible hyperfine decay paths. By quantifying the branching ratios of the $Q_{fe}(1/2)$ transitions, we propose an optical pumping protocol to accumulate population in eEDM-sensitive coherent states of $(|M_F = 1\rangle + |M_F = -1\rangle)/\sqrt{2}$, thereby amplifying the effective signal-to-noise ratio during the eEDM measurement. Hence, it is necessary to calculate the branching ratios of the selected eEDM transition of PbF molecules involving the superposition states of $(|M_F = 1\rangle + |M_F = -1\rangle)/\sqrt{2}$ and $(|M_F = 1\rangle - |M_F = -1\rangle)/\sqrt{2}$, and the upper state of $A(v' = 0, J' = 1/2, f, F' = 1, M_F' = 0)$ to figure out the feasibility of the optical pump scheme.

In the eEDM measurement, external fields including an appropriate

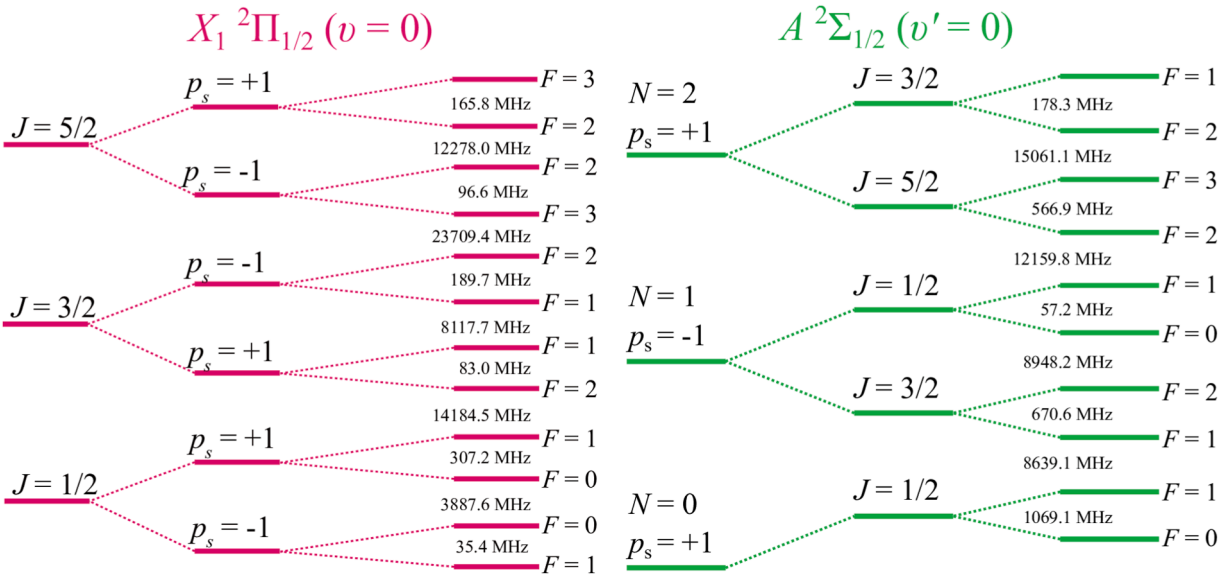

Fig. 1. The energy level structures of PbF X_1 and A states without an external electric field.

Table 1
The J-mixing of the X_1 state ($E_z = 0$ kV/cm) in the Q_{fe} (1/2) transitions. All states involved in the mixing are labeled as $|J, p_s, F, M_F\rangle$.

Mixed label	Superposition of pure J states
$\|\frac{1}{2}, 1, 0, 0\rangle$	$\|\frac{1}{2}, 1, 0, 0\rangle$
$\|\frac{1}{2}, 1, 1, -1\rangle$	$0.999997\|\frac{1}{2},1,1,-1\rangle - 0.002543\|\frac{3}{2},1,1,-1\rangle$
$\|\frac{1}{2}, 1, 1, 0\rangle$	$0.999997\|\frac{1}{2},1,1,0\rangle - 0.002543\|\frac{3}{2},1,1,0\rangle$
$\|\frac{1}{2}, 1, 1, 1\rangle$	$0.999997\|\frac{1}{2},1,1,1\rangle - 0.002543\|\frac{3}{2},1,1,1\rangle$

Table 3
The J-mixing of the A state ($|J = \frac{1}{2}, p_s = -1, F = 1, M_F = 0\rangle$) ($E_z = 0$ and 9 kV/cm) in the $Q_{fe}(1/2)$ transitions. All states are labeled as $|N, J, p_s, F, M_F\rangle$.

E_z (kV/cm)	Superposition of pure J states
0	$0.998248\|1, \frac{1}{2}, -1, 1, 0\rangle + 0.059175\|1, \frac{3}{2}, -1, 1, 0\rangle$
9	$0.947970\|1, \frac{1}{2}, -1, 1, 0\rangle + 0.233231\|0, \frac{1}{2}, 1, 0, 0\rangle -$ $0.073021\|1, \frac{3}{2}, -1, 1, 0\rangle + 0.204019\|2, \frac{3}{2}, 1, 2, 0\rangle$

electric field will be applied to investigate the evolution of the eEDM phase. When molecules pass through the applied electric and magnetic fields, different phases δ will be accumulated for the $|M_F = 1\rangle$ and $|M_F = -1\rangle$ states leading to $\left(|M_F = 1\rangle e^{-i\delta} + |M_F = -1\rangle e^{i\delta}\right)/\sqrt{2}$. The difference between the phases under two electric fields of equal intensity but opposite directions is defined as the eEDM phase δ_{eEDM} [17,64]. In the presence of a static electric field, the spherical symmetry of the system is broken due to the Stark interaction $\mathbf{H}_{\mathrm{stark}} = -\mu_e \mathbf{n}' \cdot \mathbf{E}'$, and J is no longer a good quantum number with off-diagonal elements between different J states emerging. Here, μ_e stands for molecular dipole moment of PbF, and $\mathbf{E}'$ and $\mathbf{n}'$ denote the external electric field and molecular internuclear axis with the prime sign indicating that the operators are in the molecule-base frame. Since $\mu_e \mathbf{n}'$ is a vector operator, and the associated selection rules allow $\Delta J = 0$ and ± 1, coupling between states with different J's is permitted. Consequently, the eigenstates of the full Hamiltonian are admixtures of multiple J-states [62]. Therefore, before calculating the branching ratios of transitions in $Q_{fe}(1/2)$, one must account for the J-mixing of hyperfine levels in the ground X_1 state. The mixing coefficients can be obtained by diagonalizing the effective Hamiltonian $\mathbf{H}_{\mathbf{eff}}$ introduced above. Without the external electric field, the mixing between the rotational states of X_1 in the $Q_{fe}(1/2)$ transition are shown in Table 1.

According to the results in Section 4, the $Q_{fe}(1/2)$ transition spectra will be most sensitive to the eEDM detection with an applied electric field E_z of around 9 kV/cm. Thus, the J-mixing of the hyperfine levels in the X_1 state will be calculated again under this applied electric field, which is shown in Table 2.

In addition, when calculating branching ratios, the J-mixing states in the $A(|\frac{1}{2}, -1, 1, 0\rangle)$ state under both zero external electric field and an applied electric field of 9 kV/cm (experimental condition), which is shown in Table 3, should also be considered.

Now let us discuss the calculation of the branching ratios in Hund's

Table 2
The J-mixing of the X_1 state ($E_z = 9$ kV/cm) in the Q_{fe} (1/2) transitions. All states involved in the mixing are labeled as $|J, p_s, F, M_F\rangle$.

Mixed label	Superposition of pure J states
$\|\frac{1}{2}, 1, 0, 0\rangle$	$0.492614\|\frac{1}{2}, -1, 1, 0\rangle + 0.793131\|\frac{1}{2}, 1, 0, 0\rangle + 0.256028\|\frac{3}{2}, -1, 1, 0\rangle + 0.250447\|\frac{3}{2}, 1, 2, 0\rangle$
$\|\frac{1}{2}, 1, 1, -1\rangle$	$0.479935\|\frac{1}{2},-1,1,-1\rangle + 0.799709\|\frac{1}{2},1,1,-1\rangle - 0.135295\|\frac{3}{2},-1,1,-1\rangle$ $+ 0.226407\|\frac{3}{2},-1,2,-1\rangle - 0.123292\|\frac{3}{2},1,1,-1\rangle + 0.212983\|\frac{3}{2},1,2,-1\rangle$
$\|\frac{1}{2}, 1, 1, 0\rangle$	$0.483165\|\frac{1}{2},-1,0,0\rangle + 0.798812\|\frac{1}{2},1,1,0\rangle + 0.261844\|\frac{3}{2},-1,2,0\rangle + 0.244721\|\frac{3}{2},1,1,0\rangle$
$\|\frac{1}{2}, 1, 1, 1\rangle$	$-0.479935\|\frac{1}{2},-1,1,1\rangle + 0.799709\|\frac{1}{2},1,1,1\rangle + 0.135295\|\frac{3}{2},-1,1,1\rangle$ $+ 0.226407\|\frac{3}{2},-1,2,1\rangle - 0.123292\|\frac{3}{2},1,1,1\rangle - 0.212983\|\frac{3}{2},1,2,1\rangle$

case (a) basis $|\Lambda, S, \Sigma, \Omega, J, I, F, M_F\rangle$ for the possible hyperfine decays in the $Q_{fe}(1/2)$ transition. Here, the description of the excited A states should be converted to the Hund's case (a) basis as [65]

$$|\Lambda;N,S,J,F\rangle = \sum\sum (-1)^{J+\Omega}\sqrt{2N+1}\times \begin{pmatrix} S & N & J \\ \Sigma & \Lambda & -\Omega \end{pmatrix} |\Lambda,S,\Sigma,\Omega,J,F\rangle. \quad (3)$$

The matrix elements for the electric dipole transition between two sublevels are then calculated and labeled as $|\psi_e\rangle$ and $|\psi_g\rangle$. In this frame, the electric-dipole operator is denoted as $T^{(1)}(d)$:

$$\langle d\rangle = \langle \psi_e|T^{(1)}(d)|\psi_g\rangle = (-1)^{(F_e-M_{Fe})} \begin{pmatrix} F_e & 1 & F_g \\ -M_{Fe} & p & M_{Fg} \end{pmatrix}$$

$$\times(-1)^{F_g+J_e+I_g+1}\sqrt{(2F_e+1)(2F_g+1)}\begin{Bmatrix} J_g & F_g & I_g \\ F_e & J_e & 1 \end{Bmatrix}$$

$$\times \sum_{q=-1}^{1}(-1)^{J_e-\Omega_e}\sqrt{(2J_e+1)(2J_g+1)}\begin{pmatrix} J_e & 1 & J_g \\ -\Omega_e & q & \Omega_g \end{pmatrix}$$

$$\times\langle \Lambda_e, S_e, \Sigma_e|T^{(1)}(d)|\Lambda_g, S_g, \Sigma_g\rangle. \quad (4)$$

Here the electric dipole operator $T^{(1)}(d)$ does not couple to the electron spin, and the spin projection is conserved, i.e., $\Sigma_e = \Sigma_g$. Consequently, for all the allowed $\Delta\Lambda = \pm 1$ transitions, the matrix elements $\langle \Lambda_e, S_e, \Sigma_e|T^{(1)}(d)|\Lambda_g, S_g, \Sigma_g\rangle$ remain constant and can be factored out of the summation. In our eEDM experiment, the quantization axis is defined by the direction of the applied electric field (z-axis), while the x-axis corresponds to both the propagation direction of the molecular beam and the linear polarization direction of the excitation laser. It should be emphasized that the excitation laser is assumed to be x-polarized in Eq. (4), for which the $p = \pm 1$ tensor components contribute coherently and equally. Under this condition, only transitions with $\Delta M_F = \pm 1$ are allowed. For other polarizations, such as y- or z-polarized light, the selection rules would differ, and Eq. (4) then needs to be revised accordingly. A relative electric-dipole transition matrix element between states $|\psi_e\rangle$ and $|\psi_g\rangle$ is defined as

$$r_{\psi_e,\psi_g} = \frac{\langle \psi_e|T^{(1)}(d)|\psi_g\rangle}{\langle \Lambda_e, S_e, \Sigma_e|T^{(1)}(d)|\Lambda_g, S_g, \Sigma_g\rangle}. \quad (5)$$

The manipulation of the ground state $X_1(v = 0, J = 1/2, e, F = 1, |M_F| = 1)$ will create two states defined as

$$|+\rangle = \frac{\left|J=\frac{1}{2},\ e,\ F=1,\ M_F=1\right\rangle + \left|J=\frac{1}{2},\ e,\ F=1,\ M_F=-1\right\rangle}{\sqrt{2}}, \quad (6)$$

and

$$|-\rangle = \frac{\left|J=\frac{1}{2},\ e,\ F=1,\ M_F=1\right\rangle - \left|J=\frac{1}{2},\ e,\ F=1,\ M_F=-1\right\rangle}{\sqrt{2}}. \quad (7)$$

Following the calculation procedures described above, the branching ratios of $A(|\frac{1}{2}, -1,1,0\rangle) \leftarrow X_1(|+\rangle)$ and $A(|\frac{1}{2}, -1,1,0\rangle) \leftarrow X_1(|-\rangle)$ in two different electric fields E_z of 0 and 9 kV/cm are calculated and shown in Table 4. The values listed in Table 4 are calculated based on Eq. (5), the evaluation of Eq. (6), Eq. (7), and the J-mixing results summarized in Tables 1–3.

As evident from Table 4, the branching ratio for the transitions from the $|-\rangle$ state to the upper state significantly exceeds that of the $|+\rangle$ state transitions under both field-free conditions and an applied electric field of 9 kV/cm. This asymmetry enables strategic enhancement of eEDM measurement sensitivity: by employing a laser at the frequency of the eEDM transition, the molecules in the $|-\rangle$ state are continuously pumped into the A state. Consequently, the superposition states $|+\rangle$ and $|-\rangle$, which are prepared from the degenerate states of X_1 ($v = 0$, $J = 1/2$, e, $F = 1$, $|M_F| = 1$), will be manipulated and molecules in the $|+\rangle$ state can be further enhanced as a result of repumping molecules in the A state and other associated states, thereby amplifying the population of molecules in the $|+\rangle$ state for the eEDM experiment.

4. Electric-field-dependent energy level structures and transition spectra of $Q_{fe}(1/2)$

As outlined in Section 3, the proposed eEDM measurement using PbF relies on detecting the eEDM-induced phase via the REMPI spectroscopy. The eEDM detection transition for this protocol is encompassed within the $Q_{fe}(1/2)$ transition manifold. Crucially, the application of controlled external electric field is needed to both polarize the molecules and detect the eEDM-sensitive phase evolution during the experiment. Consequently, the complete characterization of $Q_{fe}(1/2)$ energy level structures and its electric-field-dependent transition spectra is critical for the proposed eEDM measurement scheme.

To explore the field-dependent $Q_{fe}(1/2)$ transition, the interaction of the external electric field with the hyperfine levels of PbF should be investigated. As shown in Fig. 2(a), using the effective Hamiltonian approach, the evolution of $X_1(v = 0, J = 1/2, e)$ and $A(v' = 0, J' = 1/2, f)$ states under different electric fields are illustrated. Note that under the external electric field, F is not a good quantum number due to the mixing of hyperfine levels. Here, the F quantum number is used as asymptotic quantum numbers for the purpose of spectral line identification.

The energy difference between X_1 and A states at a chosen external electric field will provide information about the sensitive frequency of the $Q_{fe}(1/2)$ transitions. The theoretical $Q_{fe}(1/2)$ transition spectra under varying electric fields (Fig. 2(b)) were simulated by considering the hyperfine-resolved transition frequencies with the Boltzmann population distribution of the ground X_1 state at a rotational temperature of 5 K, combined with calculated electric dipole transition strengths. Each spectral line was modeled as a Gaussian profile with a 70 MHz full-width-at-half-maximum (FWHM), consistent with Doppler and collisional broadening under typical experimental conditions. The blue solid lines represent the complete $Q_{fe}(1/2)$ transition manifold, while the yellow dashed lines specifically identify the eEDM detection transition under different external electric fields.

In the absence of external electric fields, the eEDM detection transition remains indistinguishable from other spectral features. As the electric field strength increases, this specific transition gradually separates from neighboring transitions. Simulation reveals that at an electric field strength of 9 kV/cm, the eEDM detection transition becomes sufficiently resolved from other transitions in the $Q_{fe}(1/2)$ spectra. However, increasing further the field to 12 kV/cm induces spectral overlap

Table 4

The branching ratios of $A(|\frac{1}{2}, -1,1,0\rangle) \leftarrow X_1(|+\rangle)$ and $A(|\frac{1}{2}, -1,1,0\rangle) \leftarrow X_1(|-\rangle)$ in applied electric fields E_z of 0 and 9 kV/cm.

E_z (kV/cm)	branch ratios of $\|+\rangle$	branch ratios of $\|-\rangle$	$\frac{\text{branch ratio of } \|-\rangle}{\text{branch ratio of } \|+\rangle}$
0	0	0.423606	∞
9	0	0.263891	∞

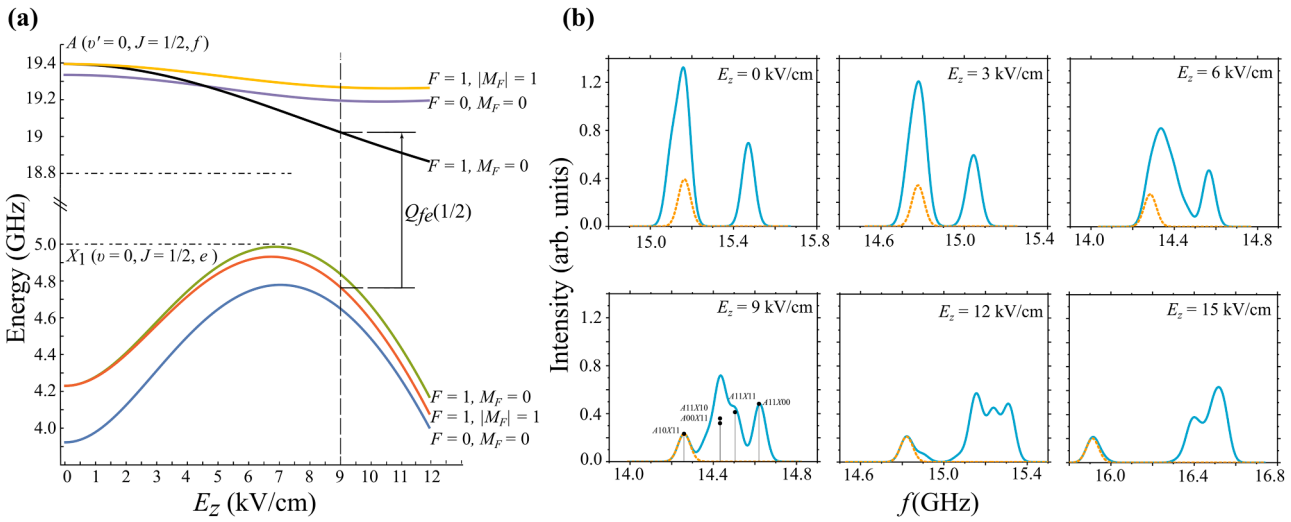

Fig. 2. (a) The energy level dependence of PbF X_1 and A states with respect to the external electric field. (b) The simulation of the Stark spectra varying from 0 to 15 kV/cm. The blue solid lines are the $Q_{fe}(1/2)$ transitions, with the yellow dashed lines indicating the specific eEDM-sensitive transition under different external electric fields. At 9 kV/cm, all transition lines are labeled with their respective positions. The annotations adjacent to each line indicate the specific transitions; for instance, "$A10X11$" denotes the transition from $X_1(F = 1, |M_F| = 1)$ to $A(F = 1, M_F = 0)$.

between the $A(|\frac{1}{2}, -1, 1, 0\rangle) \leftarrow X_1(|\frac{1}{2}, 1, 1, 0\rangle)$ transition and the eEDM detection transition. Therefore, through the complete field-dependent simulation of the $Q_{fe}(1/2)$ spectra, we identify an optimal electric field window of 9 to 12 kV/cm for the eEDM measurement.

5. Discussion

To measure the eEDM, the low-temperature PbF molecular beam can be generated via the buffer gas cooling method [66], and a highly sensitive REMPI detection scheme [67] shall be designed to measure the intensity of the eEDM transition $A(v' = 0, J' = 1/2, f, F' = 1, M_F' = 0) \leftarrow X_1(v = 0, J = 1/2, e, F = 1, |M_F| = 1)$ under different phase conditions. To improve phase sensitivity in the measurement, the precise control of the external electric field (E_z) is very important.

From Fig. 2, the eEDM transition of $A(v' = 0, J' = 1/2, f, F' = 1, M_F' = 0) \leftarrow X_1(v = 0, J = 1/2, e, F = 1, |M_F| = 1)$ is clearly isolated from the $Q_{fe}(1/2)$ transition spectra and can be easily identified with the applied electric field from 9 to 12 kV/cm. Given that the polarization factor of PbF molecules have already exceeded 90% at E_z = 8.2 kV/cm, we can apply 9 kV/cm for the eEDM measurement, which is also a more suitable value for high-voltage apparatus comparing with higher ones.

Now we can propose an all-optical measurement scheme for the eEDM measurement using PbF molecules. This proposal includes the preparation of buffer-gas cooled PbF molecular beam, and eEDM-sensitive state preparation via optical pumping from the X_1 (J = 1/2, p_s = 1, F = 1, $|M_F|$ = 1) state to the A (J = 1/2, p_s = –1, F = 1, M_F = 0) state. Due to the transition probability asymmetry between $|+\rangle$ and $|-\rangle$, the PbF molecules in the $|+\rangle$ state can be prepared selectively. After state preparation, the molecules in the $|+\rangle$ state accumulates multiple phases in an interaction region with uniform electric and magnetic fields including an eEDM phase $\delta_{eEDM} = d_{eEDM} E_{eff} \tau/\hbar$, the magnetic phase due to both background and applied magnetic fields δ_B, and other possible geometric and systematic phases δ_Ω. Here d_{eEDM} stands for the eEDM value, and τ stands for the coherent interaction time of the molecules with the electric field. Finally, PbF molecules enter the detection region, an all-optical measurement scheme along with a sensitive and efficient REMPI measurement will be performed. In detail, a 444 nm laser is modulated with an electro-optic amplitude modulator (EOAM), which adds a phase modulation δ_d to the polarization. Then, a 468 nm pico-second laser pulse drives the $A(v' = 0) \rightarrow D(v'' = 0) \rightarrow PbF^+ + e^-$ transition. Here the signal intensity is proportional to $P_{X_1 \rightarrow A} = \frac{I}{2}[1 - c \cdot \cos(2(\pm\delta_{eEDM} + \delta_B + \delta_\Omega + \delta_d))]$. By scanning δ_d via EOAM, a cosine-like curve will be generated, and the phase difference between the two curves under opposite electric field directions reveals an eEDM phase shift of $2\delta_{eEDM}$, from which the value of d_{eEDM} can be extracted.

There are other critical factors which should be considered in the eEDM measurement. The statistical uncertainty is primarily influenced by the parameters [37,68] which are shown in the Eq. (8)

$$\delta d_{eEDM} = \frac{1/\tau}{2E_{eff}\sqrt{\left(\frac{dN}{dt}\right)T}}, \tag{8}$$

where dN/dt stands for the detection rate of molecules, and T stands for the measurement time. In our designed eEDM experiment with PbF molecules, τ depends on the forward velocity of PbF molecules and the length of the interaction region. To generate the cold molecular beam with low forward velocity in the selected state, laser cooling [69–75] and Stark deceleration [76–80] techniques are widely employed. For PbF molecules, we have investigated the Franck-Condon factors for vibrational transitions of $X_2{}^2\Pi_{3/2}(v' \leq 5) \leftarrow X_1{}^2\Pi_{1/2}(v \leq 5)$, $A^2\Sigma^+(v' \leq 5) \leftarrow X_1{}^2\Pi_{1/2}(v \leq 5)$, and $B^2\Sigma^+(v' \leq 5) \leftarrow X_1{}^2\Pi_{1/2}(v \leq 5)$ by employing the Morse potential method [81,82] (Appendix C). It is evident that the $A^2\Sigma^+ \leftarrow X_1{}^2\Pi_{1/2}$ and $B^2\Sigma^+ \leftarrow X_1{}^2\Pi_{1/2}$ transitions are currently not suitable for laser cooling because of their poor diagonalization factors. For the $X_2{}^2\Pi_{3/2} \leftarrow X_1{}^2\Pi_{1/2}$ transition, it is interesting to mention that with Franck-Condon factors of $f_{00}(v' = 0 \leftarrow v = 0)$ of 0.924595, $f_{01}(v' = 0 \leftarrow v = 1)$ of 0.071711, $f_{02}(v' = 0 \leftarrow v = 2)$ of 0.003488, $f_{03}(v' = 0 \leftarrow v = 3)$ of 0.000189, and the sum $f_{00}+ f_{01}+ f_{02}+ f_{03}$ of 0.999983, PbF might be a promising candidate for laser cooling (Fig. 5). However, the long spontaneous lifetime of the upper state $X_2{}^2\Pi_{3/2}$ ($\tau_{X2}(v = 0)$ of 370 ± 40 μs) [83] limits the achievable cooling rate and pre-cooling is required to reduce the initial temperature [84]. In Fig. 2(a), the Stark energy level of the eEDM measurement state $X_1(J = 1/2, p_s = 1, F = 1, |M_F| = 1)$ (red line) is calculated. At 6.96 kV/cm, the energy of $X_1(J = 1/2, p_s = 1, F = 1, |M_F| = 1)$ reaches its maximum, and the energy difference between E_z = 6.96 kV/cm and E_z = 0 kV/cm is 2.94377 μeV. For comparison, the kinetic energy of the PbF with a velocity of 200 m/s is 0.047 eV, which is significantly larger than the energy gap. Therefore, PbF molecules in the eEDM sensitive state $X_1(J = 1/2, p_s = 1, F = 1, |M_F| = 1)$ might not be decelerated to a desired velocity via the Stark deceleration technique alone currently.

6. Summary

To conclude, we theoretically investigate the feasibility of eEDM measurement using the $^{208}Pb^{19}F$ molecule. Although further developments are required, our results suggest that PbF might be a promising candidate for the future eEDM measurement. The energy level structure, especially the hyperfine energy levels of X_1 and A states are explored by calculating the matrix elements of the effective Hamiltonian, providing a theoretical foundation for future spectroscopic measurements of the $A \leftarrow X_1$ transition in cold PbF molecules using REMPI techniques.

We further analyzed the J-mixing of the $X_1(J = 1/2, e, F = 1, |M_F| = 1)$ and $A(J' = 1/2, f, F' = 1, M_F' = 0)$ state under both 0 and 9 kV/cm, and estimated the branching ratios of $|+\rangle$ and $|-\rangle$ to the upper $A(v' = 0, J' = 1/2, f, F' = 1, M_F' = 0)$ state. Our results indicate that $|-\rangle$ is a state with transition probability much larger than that for $|+\rangle$, allowing us to selectively excite the $|-\rangle$ state with the $X_1(J = 1/2, e, F = 1, |M_F| = 1) \rightarrow A(J' = 1/2, f, F' = 1, M_F' = 0)$ transition. As a result, we can perform phase measurements on the $|+\rangle$ state without the interference from $|-\rangle$ in our eEDM experiment.

Subsequently, we explored the evolution of the eEDM-related transition $Q_{fe}(1/2)$ of PbF under external electric fields. By incorporating the population of the X_1 state and the square of the transition dipole moment, we calculated the theoretical $Q_{fe}(1/2)$ hyperfine transition spectra for a rotational temperature of 5 K and Doppler broadening of 70 MHz under different electric field conditions, which suggest an optimal external electric field of approximately 9 kV/cm.

Finally, we conducted a preliminary analysis of the feasibility of laser cooling and Stark deceleration for PbF molecules, revealing that the $A^2\Sigma^+ \leftarrow X_1{}^2\Pi_{1/2}$ and $B^2\Sigma^+ \leftarrow X_1{}^2\Pi_{1/2}$ transitions are not suitable for laser cooling due to their poorly diagonal Franck-Condon factors. The $X_2{}^2\Pi_{3/2} \leftarrow X_1{}^2\Pi_{1/2}$ transition, on the other hand, may be suitable for laser cooling in theory, but the long spontaneous radiation lifetime of the upper state poses a significant challenge. Additionally, we found that Stark deceleration of the eEDM measurement state $X_1(J = 1/2, p_s = 1, F = 1, |M_F| = 1)$ is not feasible since the Stark shift at the turning point of the potential is much smaller than the kinetic energy of the PbF molecule at 200 m/s.

Our work therefore establishes a comprehensive framework for the eEDM measurement using $^{208}Pb^{19}F$ molecules. These theoretical investigations, when integrated with cryogenic molecular beam technologies, position PbF as a promising tabletop platform for probing CP violation and other new physics beyond the Standard Model.

CRediT authorship contribution statement

Zesen Wang: Methodology, Software, Validation, Formal analysis, Investigation, Data curation, Writing – original draft, Writing – review & editing, Visualization. **Renjun Pang:** Validation, Investigation. **Jie Ma:** Validation, Investigation. **Qinning Lin:** Validation, Investigation. **Yabing Ji:** Validation, Investigation. **Shunyong Hou:** Validation, Investigation. **Xiaohu Li:** Investigation, Funding acquisition. **Liang Xu:** Validation, Formal analysis, Investigation. **Xingjia Li:** Validation, Formal analysis, Investigation. **Guanglong Chen:** Validation, Investigation. **Zhenghai Yang:** Validation, Investigation, Writing – review & editing, Supervision. **Jianping Yin:** Validation, Investigation. **Tao Yang:** Conceptualization, Methodology, Investigation, Resources, Writing – review & editing, Supervision, Project administration, Funding acquisition.

Declaration of competing interest

The authors declare that they have no known competing financial interests or personal relationships that could have appeared to influence the work reported in this paper.

Acknowledgments

Our work is supported by the National Natural Science Foundation of China (Grants Nos. 12274140, 12034008, 12250003, 12204308, 12304310, 12174247, and 92461301), the Program for Professor of Special Appointment (Eastern Scholar) at Shanghai Institutions of Higher Learning, the Young Top Notch Talent Support Program of Shanghai, the Xinjiang Tianchi Talent Program (2023), the Shanghai Natural Science Foundation (Grant No. 22ZR1421400), and Science and Technology Commission of Shanghai Municipality (22ZR1444100). X. H.L. acknowledges support from the Natural Science Foundation of Xinjiang Uygur Autonomous Region (No. 2024D01E37).

Appendix A. Matrix representations for the effective Hamiltonian

The spin-rotational Hamiltonian $\mathbf{H_{rot}}$ is different in X_1 and A states. In the X_1 state, the matrix of $\mathbf{H}_{\mathbf{rot},X_1}$ can be described as [62]:

$$\langle F', I', J', M_F', p_s' | \mathbf{H}_{\mathbf{rot},X_1} | F, I, J, M, p_s \rangle = \delta_{FF'} \delta_{II'} \delta_{JJ'} \delta_{M_F M_F'} \delta_{p_s p_s'} U_-(J, p_s), \tag{A1}$$

where $U_-(J,p_s)$ is given by the lower eigenvalue of Eq. (1) in the Ref. [62]. In the A state, the matrix of $\mathbf{H}_{\mathbf{rot},A}$ can be described as [59,60]:

$$\langle F', I', J', M_F', p_s' | \mathbf{H}_{\mathbf{rot},A} | F, I, J, M_F, p_s \rangle$$

$$= \delta_{JJ'} \delta_{FF'} \delta_{M_F M_F'} \delta_{II'} \delta_{p_s p_s'} \left(T_v + BJ(J+1) - DJ^2(J+1)^2 + \frac{p_s}{2}(-1)^{J+\frac{1}{2}} \left(p\left(J+\frac{1}{2}\right) + p_D\left(J+\frac{1}{2}\right)^3 \right) \right). \tag{A2}$$

For $^{208}Pb^{19}F$, the nuclear spin of the lead nucleus and the fluorine nucleus are $I_{Pb} = 0$ and $I_1 = I_F = 1/2$. The Hamiltonians $\mathbf{H_0}$, $\mathbf{H_1}$, and $\mathbf{H_{stark}}$ are the same for the X_1 and A states of $^{208}Pb^{19}F$, which are listed as follows:

$$\mathbf{H}_0 = \mathbf{I}_1' \cdot \widehat{A}_1 \cdot \mathbf{S}', \tag{A3}$$

$$\mathbf{H}_1 = c_1 \mathbf{I}_1 \cdot \mathbf{J} + (d_{c_1} \mathbf{I}_1 \cdot \mathbf{J})(\mathbf{J}' \cdot \mathbf{S}'), \tag{A4}$$

$$\mathbf{H}_{\text{stark}} = -\mu_e \mathbf{n}' \cdot \mathbf{E}'. \tag{A5}$$

The matrix elements of these three Hamiltonians have already been listed in the Ref. [62].

Appendix B. Parameters for the $^{208}Pb^{19}F$ molecule

Table 5
Parameters of $X_1^2\Pi_{1/2}(v = 0)$ state (Units in MHz if not stated).

Parameter	Description	Value
A	Spin-orbit parameter	248116740(2)[a]
$\widetilde{A}_H$	Spin-orbit dependent correction to D	0.0000897(6)[a]
$\widetilde{A}_D$	Spin-orbit dependent correction to B	157.5952(40)[a]
B	Rotational constant	6915.1148(20)[a]
D	Centrifugal correction to the rotational constant	0.005476(7)[a]
p	Ω-doubling parameter	-4143.54907(30)[a]
p_D	Centrifugal correction to the Ω-doubling parameter	-0.00314(3)[a]
$A_{\parallel 1}$	Hyperfine parallel constant of nucleus fluorine	409.906(1)[a]
$A_{\perp 1}$	Hyperfine perpendicular constant of nucleus fluorine	255.9909(7)[a]
c_1	Nuclear-spin-rotational interaction term $c_1\mathbf{I}_1 \cdot \mathbf{J}$	0.0093(2)[a]
d_{c_1}	Nuclear-rotational correction parameter	0.00056(10)[a]
μ_e (Debye)	Molecular dipole moment	3.5(3)[a]

[a] From Ref. [62].

Table 6
Parameters of $A^2\Sigma_{1/2}(v' = 0)$ state.

Parameter	Description	Value
T_v (cm^{-1})	Band origin for $A(v' = 0) \leftarrow X_1(v = 0)$	22502.09(1)[a]
B (cm^{-1})	Rotational constant	0.20691(4)[a]
10^7D (cm^{-1})	Centrifugal correction to the rotational constant	2.23(3)[a]
p (cm^{-1})	Ω-doubling parameter	0.6185(3)[a]
10^7p_D (MHz)	Centrifugal correction to the Ω-doubling parameter	-10.2(4)[a]
$A_{\parallel 1}$ (GHz)	Hyperfine parallel constant of nucleus fluorine	1.640(70)[b]
$A_{\perp 1}$ (GHz)	Hyperfine parallel constant of nucleus fluorine	0.785(18)[b]
μ_e (Debye)	Molecular dipole moment	2.8(2)[c]

[a] From Ref. [60].
[b] From Ref. [67], $A^2\Sigma_{1/2}(v' = 1)$ data.
[c] From Ref. [62], $A^2\Sigma_{1/2}(v' = 1)$ data.

Appendix C. Franck-Condon Factor of $^{208}Pb^{19}F$

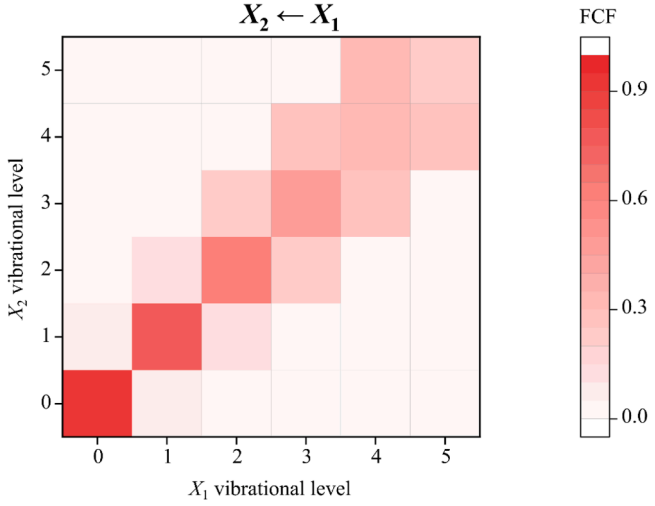

Fig. 3. Franck-Condon factors for vibrational transitions of $X_2{}^2\Pi_{3/2}$ $(v' \leq 5) \leftarrow X_1{}^2\Pi_{1/2}$ $(v \leq 5)$.

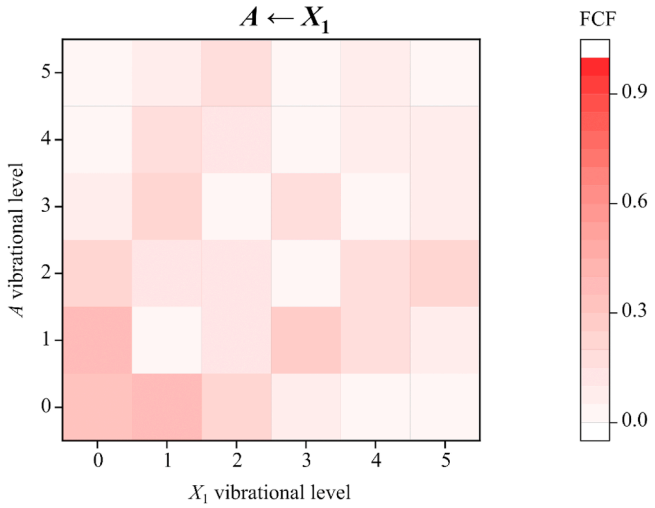

Fig. 4. Franck-Condon factors for vibrational transitions of $A^2\Sigma^+$ ($v' \leq 5$) ← $X_1{}^2\Pi_{1/2}$ ($v \leq 5$).

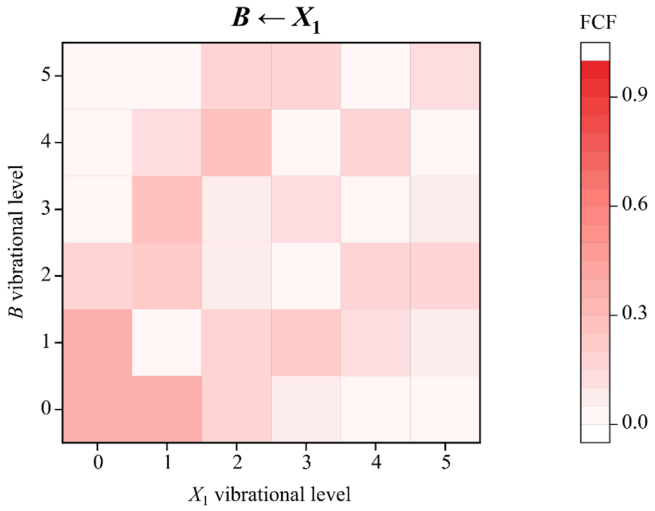

Fig. 5. Franck-Condon factors for vibrational transitions of $B^2\Sigma^+$ ($v' \leq 5$) ← $X_1{}^2\Pi_{1/2}$ ($v \leq 5$).

Data availability

No data was used for the research described in the article.

References

[1] Purcell EM, Ramsey NF. On the Possibility of Electric Dipole Moments for Elementary Particles and Nuclei. Phys Rev 1950;78:807. https://doi.org/10.1103/PhysRev.78.807.

[2] Morrissey DE, Ramsey-Musolf MJ. Electroweak baryogenesis. New J Phys 2012;14:125003. https://doi.org/10.1088/1367-2630/14/12/125003.

[3] Collaboration Planck, R Adam, Ade PAR, Aghanim N, Akrami Y, Alves MIR, et al. Planck 2015 results: I. Overview of products and scientific results. A&A 2016;594:A1. https://doi.org/10.1051/0004-6361/201527101.

[4] Pospelov M, Ritz A. Electric dipole moments as probes of new physics. Ann. Phys. 2005;318:119–69. https://doi.org/10.1016/j.aop.2005.04.002.

[5] Kara DM, Smallman IJ, Hudson JJ, Sauer BE, Tarbutt MR, Hinds EA. Measurement of the electron's electric dipole moment using YbF molecules: methods and data analysis. New J Phys 2012;14:103051. https://doi.org/10.1088/1367-2630/14/10/103051.

[6] Pendlebury JM, Hinds EA. Particle electric dipole moments. Nucl. Instrum. Methods Phys. Res. A 2000;440:471–8. https://doi.org/10.1016/S0168-9002(99)01023-2.

[7] Hinds EA. Testing time reversal symmetry using molecules. Phys Scr 1997;T70:34–41. https://doi.org/10.1088/0031-8949/1997/T70/005.

[8] Sandars PGH. Electric dipole moments of charged particles. Contemporary Physics 2001;42:97–111. https://doi.org/10.1080/00107510010027781.

[9] Commins ED, Jackson JD, DeMille DP. The electric dipole moment of the electron: An intuitive explanation for the evasion of Schiff's theorem. Am. J. Phys. 2007;75:532–6. https://doi.org/10.1119/1.2710486.

[10] Nir Y. CP violation in and beyond the standard model. In: Proceedings, 27th SLAC Summer Institute on Particle Physics: CP Violation in and Beyond the Standard Model (SSI 99); 1999. p. 165–243.

[11] Fukuyama T. Searching for new physics beyond The Standard Model In Electric Dipole Moment. Int J Mod Phys A 2012;27:1230015. https://doi.org/10.1142/S0217751X12300153.

[12] Ellis SAR, Kane GL. Theoretical prediction and impact of fundamental electric dipole moments. J High Energ Phys 2016:77. https://doi.org/10.1007/JHEP01(2016)077. 2016.

[13] Orzel C. Measuring (almost) zero. Phys World 2009;22:23–7. https://doi.org/10.1088/2058-7058/22/12/31.

[14] Regan BC, Commins ED, Schmidt CJ, DeMille D. New Limit on the Electron Electric Dipole Moment. Phys Rev Lett 2002;88:071805. https://doi.org/10.1103/PhysRevLett.88.071805.

[15] Hudson JJ, Kara DM, Smallman IJ, Sauer BE, Tarbutt MR, Hinds EA. Improved measurement of the shape of the electron. Nature 2011;473:493–6. https://doi.org/10.1038/nature10104.

[16] Collaboration The ACME, Baron J, Campbell WC, DeMille D, Doyle JM, Gabrielse G, et al. Order of Magnitude Smaller Limit on the Electric Dipole Moment of the Electron. Science 2014;343:269–72. https://doi.org/10.1126/science.1248213.

[17] Collaboration ACME. Improved limit on the electric dipole moment of the electron. Nature 2018;562:355–60. https://doi.org/10.1038/s41586-018-0599-8.

[18] Roussy TS, Caldwell L, Wright T, Cairncross WB, Shagam Y, Ng KB, et al. An improved bound on the electron's electric dipole moment. Science 2023;381:46–50. https://doi.org/10.1126/science.adg4084.

[19] Inoue T, Ando S, Aoki T, Arikawa H, Ezure S, Harada K, et al. Experimental search for the electron electric dipole moment with laser cooled francium atoms. Hyperfine Interact 2015;231:157–62. https://doi.org/10.1007/s10751-014-1100-1.

[20] Zhu K. Measuring the electron electric dipole moment using laser-cooled cesium atoms in optical lattices. Ph.D. The Pennsylvania State University; 2013.

[21] Tang C, Zhang T, Weiss DS. Improving sensitivity to magnetic fields and electric dipole moments by using measurements of individual magnetic sublevels. Phys Rev A 2018;97:033404. https://doi.org/10.1103/PhysRevA.97.033404.

[22] Zhang T. An Improved Measurement of Cesium Ground State Tensor Polarizability. Ph.D. The Pennsylvania State University; 2021.

[23] Kim YJ, Liu C-Y, Lamoreaux SK, Visser G, Kunkler B, Matlashov AN, et al. New experimental limit on the electric dipole moment of the electron in a paramagnetic insulator. Phys Rev D 2015;91:102004. https://doi.org/10.1103/PhysRevD.91.102004.

[24] Sushkov AO, Eckel S, Lamoreaux SK. Prospects for a new search for the electron electric-dipole moment in solid gadolinium-iron-garnet ceramics. Phys Rev A 2009;79:022118. https://doi.org/10.1103/PhysRevA.79.022118.

[25] Koyanagi GK, Lambo RL, Ragyanszki A, Fournier R, Horbatsch M, Hessels EA. Accurate calculation of the interaction of a barium monofluoride molecule with an argon atom: A step towards using matrix isolation of BaF for determining the electron electric dipole moment. J. Mol. Spectrosc. 2023;391:111736. https://doi.org/10.1016/j.jms.2023.111736.

[26] Lambo RL, Koyanagi GK, Horbatsch M, Fournier R, Hessels EA. Calculation of the local environment of a barium monofluoride molecule in a neon matrix. Mol. Phys. 2023;121:e2232051. https://doi.org/10.1080/00268976.2023.2232051.

[27] Lambo RL, Koyanagi GK, Ragyanszki A, Horbatsch M, Fournier R, Hessels EA. Calculation of the local environment of a barium monofluoride molecule in an argon matrix: a step towards using matrix-isolated BaF for determining the electron electric dipole moment. Mol. Phys. 2023;121:e2198044. https://doi.org/10.1080/00268976.2023.2198044.

[28] Vutha A, Horbatsch M, Hessels E. Oriented Polar Molecules in a Solid Inert-Gas Matrix: A Proposed Method for Measuring the Electric Dipole Moment of the Electron. Atoms 2018;6:3. https://doi.org/10.3390/atoms6010003.

[29] Gresh DN, Cossel KC, Zhou Y, Ye J, Cornell EA. Broadband velocity modulation spectroscopy of ThF^+ for use in a measurement of the electron electric dipole moment. J. Mol. Spectrosc. 2016;319:1–9. https://doi.org/10.1016/j.jms.2015.11.001.

[30] Zhou Y, Ng KB, Cheng L, Gresh DN, Field RW, Ye J, et al. Visible and ultraviolet laser spectroscopy of ThF. J. Mol. Spectrosc. 2019;358:1–16. https://doi.org/10.1016/j.jms.2019.02.006.

[31] Zhou Y, Shagam Y, Cairncross WB, Ng KB, Roussy TS, Grogan T, et al. Second-Scale Coherence Measured at the Quantum Projection Noise Limit with Hundreds of Molecular Ions. Phys Rev Lett 2020;124:053201. https://doi.org/10.1103/PhysRevLett.124.053201.

[32] Ng KB, Zhou Y, Cheng L, Schlossberger N, Park SY, Roussy TS, et al. Spectroscopy on the electron-electric-dipole-moment–sensitive states of ThF^+. Phys Rev A 2022;105:022823. https://doi.org/10.1103/PhysRevA.105.022823.

[33] Zhou Y, Island JO, Grau M. Quantum logic control and precision measurements of molecular ions in a ring trap: An approach for testing fundamental symmetries. Phys Rev A 2024;109:033107. https://doi.org/10.1103/PhysRevA.109.033107.

[34] Oleynichenko AV, Skripnikov LV, Zaitsevskii AV, Flambaum VV. Laser-coolable $AcOH^+$ ion for CP-violation searches. Phys Rev A 2022;105:022825. https://doi.org/10.1103/PhysRevA.105.022825.

[35] Maison DE, Skripnikov LV, Penyazkov G, Grau M, Petrov ANT. P-odd effects in the $LuOH^+$ cation. Phys Rev A 2022;106:062827. https://doi.org/10.1103/PhysRevA.106.062827.

[36] Kurchavov I, Maison D, Skripnikov L, Grau M, Petrov A. Nuclear magnetic quadrupole moment of ^{175}Lu and parity-violating polarization degree of levels in $^{175}LuOH^+$. Phys Rev A 2023;108:052815. https://doi.org/10.1103/PhysRevA.108.052815.

[37] The NL-eEDM collaboration Aggarwal P, Bethlem HL, Borschevsky A, Denis M, Esajas K, et al. Measuring the electric dipole moment of the electron in BaF. Eur Phys J D 2018;72:197. https://doi.org/10.1140/epjd/e2018-90192-9.

[38] Haase PAB, Doeglas DJ, Boeschoten A, Eliav E, Iliaš M, Aggarwal P, et al. Systematic study and uncertainty evaluation of P, T-odd molecular enhancement factors in BaF. J Chem Phys 2021;155:034309. https://doi.org/10.1063/5.0047344.

[39] Talukdar K, Nayak MK, Vaval N, Pal S. Relativistic coupled-cluster study of BaF in search of CP violation. J Phys B: At Mol Opt Phys 2020;53:135102. https://doi.org/10.1088/1361-6455/ab84c8.

[40] Sabor S, Fadili D, Touimi Benjelloun A, Benzakour M, Mcharfi M. Computational spectroscopy of diatomic tungsten carbide. WC. J. Mol. Spectrosc. 2020;371:111305. https://doi.org/10.1016/j.jms.2020.111305.

[41] Lee J, Chen J, Skripnikov LV, Petrov AN, Titov AV, Mosyagin NS, et al. Optical spectroscopy of tungsten carbide for uncertainty analysis in electron electric-dipole-moment search. Phys Rev A 2013;87:022516. https://doi.org/10.1103/PhysRevA.87.022516.

[42] Lee J, Meyer ER, Paudel R, Bohn JL, Leanhardt AE. An electron electric dipole moment search in the $X^3\Delta_1$ ground state of tungsten carbide molecules. J. Mod. Opt. 2009;56:2005–12. https://doi.org/10.1080/09500340903349930.

[43] Isaev TA, Hoekstra S, Berger R. Laser-cooled RaF as a promising candidate to measure molecular parity violation. Phys Rev A 2010;82:052521. https://doi.org/10.1103/PhysRevA.82.052521.

[44] Fazil NM, Prasannaa VS, Latha KVP, Abe M, Das BP. RaH as a potential candidate for electron electric-dipole-moment searches. Phys Rev A 2019;99:052502. https://doi.org/10.1103/PhysRevA.99.052502.

[45] Prasannaa VS, Vutha AC, Abe M, Das BP. Mercury Monohalides: Suitability for Electron Electric Dipole Moment Searches. Phys Rev Lett 2015;114:183001. https://doi.org/10.1103/PhysRevLett.114.183001.

[46] Sasmal S, Pathak H, Nayak MK, Vaval N, Pal S. Search for parity and time reversal violating effects in HgH: Relativistic coupled-cluster study. The J. Chem. Phys. 2016;144:124307. https://doi.org/10.1063/1.4944673.

[47] Talukdar K, Nayak MK, Vaval N, Pal S. Role of electron correlation in the P, T-odd effects of CdH: A relativistic coupled-cluster investigation. Phys Rev A 2020;101:032505. https://doi.org/10.1103/PhysRevA.101.032505.

[48] Mitra R, Prasannaa VS, Ruiz RFG, Sato TK, Abe M, Sakemi Y, et al. Towards CP-violation studies on superheavy molecules: Theoretical and experimental perspectives. Phys Rev A 2021;104:062801. https://doi.org/10.1103/PhysRevA.104.062801.

[49] Yang Z, Li J, Lin Q, Xu L, Wang H, Yang T, et al. Laser-cooled HgF as a promising candidate to measure the electric dipole moment of the electron. Phys Rev A 2019;99:032502. https://doi.org/10.1103/PhysRevA.99.032502.

[50] Kozyryev I, Hutzler NR. Precision Measurement of Time-Reversal Symmetry Violation with Laser-Cooled Polyatomic Molecules. Phys Rev Lett 2017;119:133002. https://doi.org/10.1103/PhysRevLett.119.133002.

[51] Prasannaa VS, Shitara N, Sakurai A, Abe M, Das BP. Enhanced sensitivity of the electron electric dipole moment from YbOH: The role of theory. Phys Rev A 2019;99:062502. https://doi.org/10.1103/PhysRevA.99.062502.

[52] Mitra R, Prasannaa VS, Sahoo BK, Hutzler NR, Abe M, Das BP. Study of HgOH to Assess Its Suitability for Electron Electric Dipole Moment Searches. Atoms 2021;9:7. https://doi.org/10.3390/atoms9010007.

[53] Augenbraun BL, Lasner ZD, Frenett A, Sawaoka H, Le AT, Doyle JM, et al. Observation and laser spectroscopy of ytterbium monomethoxide, $YbOCH_3$. Phys Rev A 2021;103:022814. https://doi.org/10.1103/PhysRevA.103.022814.

[54] Zakharova A. Rotating and vibrating symmetric-top molecule $RaOCH_3$ in fundamental P, T-violation searches. Phys Rev A 2022;105:032811. https://doi.org/10.1103/PhysRevA.105.032811.

[55] Shafer-Ray NE. Possibility of 0-g-factor paramagnetic molecules for measurement of the electron's electric dipole moment. Phys Rev A 2006;73:034102. https://doi.org/10.1103/PhysRevA.73.034102.

[56] Baklanov KI, Petrov AN, Titov AV, Kozlov MG. Progress toward the electron electric-dipole-moment search: Theoretical study of the PbF molecule. Phys Rev A 2010;82:060501. https://doi.org/10.1103/PhysRevA.82.060501.

[57] Das KK, Petsalakis ID, Liebermann H-P, Alekseyev AB, Buenker RJ. Ab initio spin-orbit CI calculations of the potential curves and radiative lifetimes of low-lying states of lead monofluoride. J. Chem. Phys. 2002;116:608–16. https://doi.org/10.1063/1.1423944.

[58] Sivakumar P, McRaven CP, Rupasinghe PM, TZh Yang, Shafer-Ray NE, Sears TJ, et al. Pseudo-continuous resonance enhanced multiphoton ionisation: application to the determination of the hyperfine constants of $^{208}Pb^{19}F$. Mol. Phys. 2010;108:927–35. https://doi.org/10.1080/00268970903567304.

[59] McRaven CP. Study of the lead monofluoride molecule in preparation of a measurement of the electric dipole moment of the electron. Doctor of Philosophy. University of Oklahoma; 2010.

[60] Lumley DJW, Barrow RF. Rotational analysis of the B-X_2, B-X_1 and A-X_1 systems of gaseous PbF. J Phys B: At Mol Phys 1977;10:1537–41. https://doi.org/10.1088/0022-3700/10/8/025.

[61] McRaven CP, Sivakumar P, Shafer-Ray NE, Hall GE, Sears TJ. Spectroscopic constants of the known electronic states of lead monofluoride. J. Mol. Spectrosc. 2010;262:89–92. https://doi.org/10.1016/j.jms.2010.05.006.

[62] Mawhorter RJ, Murphy BS, Baum AL, Sears TJ, Yang T, Rupasinghe PM, et al. Characterization of the ground X_1 state of $^{204}Pb^{19}F$, $^{206}Pb^{19}F$, $^{207}Pb^{19}F$, and $^{208}Pb^{19}F$. Phys Rev A 2011;84:022508. https://doi.org/10.1103/PhysRevA.84.022508.

[63] Frosch RA, Foley HM. Magnetic Hyperfine Structure in Diatomic Molecules. Phys Rev 1952;88:1337–49. https://doi.org/10.1103/PhysRev.88.1337.

[64] Fortson N, Sandars P, Barr S. The Search for a Permanent Electric Dipole Moment. Physics Today 2003;56:33–9. https://doi.org/10.1063/1.1595052.

[65] Chen T, Bu W, Yan B. Structure, branching ratios, and a laser-cooling scheme for the ^{138}BaF molecule. Phys Rev A 2016;94:063415. https://doi.org/10.1103/PhysRevA.94.063415.

[66] Wang Z, Pang R, Ma J, Lin Q, Hou S, Wang H, et al. Spectroscopic characterization of buffer-gas-cooled lead monofluoride molecules in the $B\ ^2\Sigma^+(v' = 0) \leftarrow X_1\ ^2\Pi_{1/2}(v = 0)$ transition. Spectrochim. Acta A Mol. Biomol. Spectrosc. 2025;329:125508. https://doi.org/10.1016/j.saa.2024.125508.

[67] Sivakumar P, McRaven CP, Rupasinghe PM, TZh Yang, Shafer-Ray NE, Sears TJ, et al. Pseudo-continuous resonance enhanced multiphoton ionisation: application to the determination of the hyperfine constants of $^{208}Pb^{19}F$. Mol. Phys. 2010;108:927–35. https://doi.org/10.1080/00268970903567304.

[68] Vutha AC, Campbell WC, Gurevich YV, Hutzler NR, Parsons M, Patterson D, et al. Search for the electric dipole moment of the electron with thorium monoxide. J Phys B: At Mol Opt Phys 2010;43:074007. https://doi.org/10.1088/0953-4075/43/7/074007.

[69] Pang R, Yin J, Wang Y, Lin Q, Wang Z, Xu L, et al. Theoretical Investigation of Spectroscopic Properties of the Alkaline-Earth-Metal Monohydrides toward Laser Cooling and Magneto-Optical Trapping. ACS Omega 2023;8:19391–401. https://doi.org/10.1021/acsomega.3c00352.

[70] Xia M, Yin Y, Pei C, Ye Y, Gu R, Yan K, et al. A crossed focused vortex beam with application to cold molecules*. Chinese Phys B 2021;30:114202. https://doi.org/10.1088/1674-1056/abf915.
[71] Xia M, Gu R, Yan K, Wu D, Xu L, Xia Y, et al. Destabilization of dark states in MgF molecules. Phys Rev A 2021;103:013321. https://doi.org/10.1103/PhysRevA.103.013321.
[72] Gu R, Xia M, Yan K, Wu D, Wei J, Xu L, et al. Rotational analysis and hyperfine structures of $A^2\Pi_{1/2} \rightarrow X^2\Sigma_{1/2}$ transition in ^{25,26}MgF isotope molecules. J. Quant. Spectrosc. Radiat. Transf. 2022;278:108015. https://doi.org/10.1016/j.jqsrt.2021.108015.
[73] Gu R, Yan K, Wu D, Wei J, Xia Y, Yin J. Radiative force from optical cycling on magnesium monofluoride. Phys Rev A 2022;105:042806. https://doi.org/10.1103/PhysRevA.105.042806.
[74] Yan K, Wei B, Yin Y, Xu S, Xu L, Xia M, et al. A new route for laser cooling and trapping of cold molecules: Intensity-gradient cooling of MgF molecules using localized hollow beams. New J Phys 2020;22:033003. https://doi.org/10.1088/1367-2630/ab7253.
[75] Yan K, Gu R, Wu D, Wei J, Xia Y, Yin J. Simulation of EOM-based frequency-chirped laser slowing of MgF radicals. Front Phys 2022;17:42502. https://doi.org/10.1007/s11467-021-1137-y.
[76] Ji Y, Liu Q, Liu Y, Yang T, Hou S, Yin J. Design of a ring-shaped traveling-wave Zeeman decelerator for both light and heavy molecules. Phys Rev A 2023;108:043115. https://doi.org/10.1103/PhysRevA.108.043115.
[77] Guo H, Ji Y, Liu Q, Yang T, Hou S, Yin J. A driven three-dimensional electric lattice for polar molecules. Front Phys 2022;17:52505. https://doi.org/10.1007/s11467-022-1174-1.
[78] Guo H, Ji Y, Liu Q, Yang T, Hou S, Yin J. Controllable three-dimensional electrostatic lattices for manipulation of cold polar molecules. Phys Rev A 2022;105:053108. https://doi.org/10.1103/PhysRevA.105.053108.
[79] Ji Y-B, Wei B, Guo H-J, Liu Q, Yang T, Hou S-Y, et al. Formation of high-density cold molecules via electromagnetic trap. Chinese Phys B 2022;31:103201. https://doi.org/10.1088/1674-1056/ac720c.
[80] Wei B, Guo H, Ji Y, Yang T, Hou S, Yin J. A scalable two-dimensional moving electric lattice on a chip for polar molecules. Opt. Commun. 2020;475:126208. https://doi.org/10.1016/j.optcom.2020.126208.
[81] Ley-Koo E, Mateos-Cortés S, Villa-Torres G. Vibrational levels and Franck–Condon factors of diatomic molecules via Morse potentials in a box. Int J of Quantum Chemistry 1995;56:175–86. https://doi.org/10.1002/qua.560560305.
[82] Matsumoto A, Iwamoto K. Analytical formula for Franck-Condon factors involving the Morse potential. J. Quant. Spectrosc. Radiat. Transf. 1993;50:103–9. https://doi.org/10.1016/0022-4073(93)90133-3.
[83] Shestakov O, Pravilov AM, Demes H, Fink EH. Radiative lifetime and quenching of the A $^2\Sigma^+$ and X_2 $^2\Pi_{3/2}$ states of PbF. Chem. Phys. 1992;165:415–27. https://doi.org/10.1016/0301-0104(92)87056-F.
[84] Luan J-Z, Yang C-L, Li X, Liu W-W, Liu Y-L, Zhao W-K. Spectroscopic properties and laser cooling feasibility with the $X_1{}^2\Pi_{1/2} \leftrightarrow X_2{}^2\Pi_{3/2}$ transition for the PbX (X = F, Cl, Br, and I) molecules. Phys Scr 2024;99:035406. https://doi.org/10.1088/1402-4896/ad23b3.